Site-Sensitive Selective CO₂ Photoreduction to CO over Gold Nanoparticles

Haowei Huang,[1,#] Jiwu Zhao,[2,#] Chen Zhou,[3] Feili Lai,[4] Menglong Zhang,[5] Bo Weng,[1,*] Jinlin Long,[2,*] Johan Hofkens,[4,6] Maarten B. J. Roeffaers,[1] Julian A. Steele[1,*]

1) cMACS, Department of Microbial and Molecular Systems KU Leuven, Celestijnenlaan 200F, 3001 Leuven, Belgium

2) State Key Lab of Photocatalysis on Energy and Environment, College of Chemistry, Fuzhou University, Fuzhou, 350116, P. R. China

3) College of Chemical Engineering, Fuzhou University, Fuzhou, 350116, P. R. China

4) Department of Chemistry, Faculty of Sciences, KU Leuven, Celestijnenlaan 200F, 3001 Leuven, Belgium

5) Institute of Semiconductors, South China Normal University, Guangzhou 510631 China

6) Max Planck Institute for Polymer Research, Ackermannweg 10, 55128 Mainz, Germany

# these authors are contribution equally.

E-mail: bo.weng@kuleuven.be; jllong@fzu.edu.cn; julian.steele@kuleuven.be

Abstract: The work demonstrated a new case of materials-gene engineering to precisely design photocatalysts with the prescribed properties. On the base of DFT calculations, a phase-doping strategy was proposed to regulate the pathways of CO_2 conversion over Au nanoparticles (NPs) loaded TiO_2 photocatalysts. As a result, the thermodynamic bottleneck of CO_2-to-CO conversion was successfully unlocked by the incorporation of stable twinning crystal planes into *fcc*-phase Au NPs. The activity results showed that compared to bare pristine TiO_2, the loading of regular *fcc*-Au NPs raised the CO production by 18-fold but suppressed the selectivity from 84% to 75%, whereas Au NPs with twinning (110) and (100) facets boosted the activity by nearly 40-fold and established near unity CO selectivity. It was well established that this enhancement was originated from a beneficial shift in the surface reactive site energetics arising at the twinned stacking fault, whereby both the CO reaction energy and desorption energy were significantly reduced.

Solar-driven CO_2 conversion presents a promisingly effective approach to support a more sustainable global carbon cycle.[1] The most reported CO_2 reduction products in photocatalytic reactions are CH_4 and CO.[2] CH_4 is naturally abundant (i.e. the main component of natural gas, shale gas and flammable ice) and often used in the energy-intensive production of syngas (the mixture of CO and H_2) through steam reforming.[3] Syngas is industrially important, as it forms the starting point for the production of various base chemicals, i.e., methanol and other commodity hydrocarbons. The conversion of CO_2 to CH_4 is an eight-electron reduction which is kinetically unfavored compared to CO production which requires two electrons.[4] Therefore, the direct photoreduction of CO_2 into CO, rather than CH_4, is arguably the technologically and economically preferred approach. Indeed, directly converting CO_2 into C_{2+} hydrocarbons is a more preferable route.[5] However, it is still challenging with high effiency and selectivity.

An effective strategy for reducing CO_2 to CO with high selectivity is to engineer an appropriate catalyst stabilizing the reaction intermediates leading to CO, rather than CH_4. A suitable co-catalyst should accelerate the photo-promoted charge transfer, lower the overall CO_2 activation energy, increase the surface catalytic reaction rate and, thus, maximize the solar-to-chemical energy conversion efficiency.[4a] Among the various metal co-catalysts on offer, Au NPs have been widely utilized to improve the photocatalytic performance, due to their attractive electronic, optical and catalytic features when formed into NPs, such as empty antibonding orbitals, electron sink, surface plasmons.[6] However,

it has been well-documented in most publications that CO_2 underwent the multiple hydrogenation on either the C atom or the O atoms via the proton-coupled electron transfer (PCET) processes.[4] The hydrogenation on the C atom, which generated finally CH_4 via the HCOO* formation ($CO_2 + 8H^+ + 8e^- \rightarrow CH_4 + 2H_2O$, Eq. 1), was thermodynamically more favorable than that on the O atoms ($CO_2 + H^+ + e^- \rightarrow COOH*$, Eq. 2). In most cases, the selectivity towards the desired products can be steered by the first hydrogenation over *fcc*-phase Au NPs loaded semiconductor catalysts (Figure 1a). Therefore, from a thermodynamic viewpoint, reducing the Gibbs energy barrier of the Eq. 2 reaction should be obligatory to achieve the target CO_2-to-CO conversion.
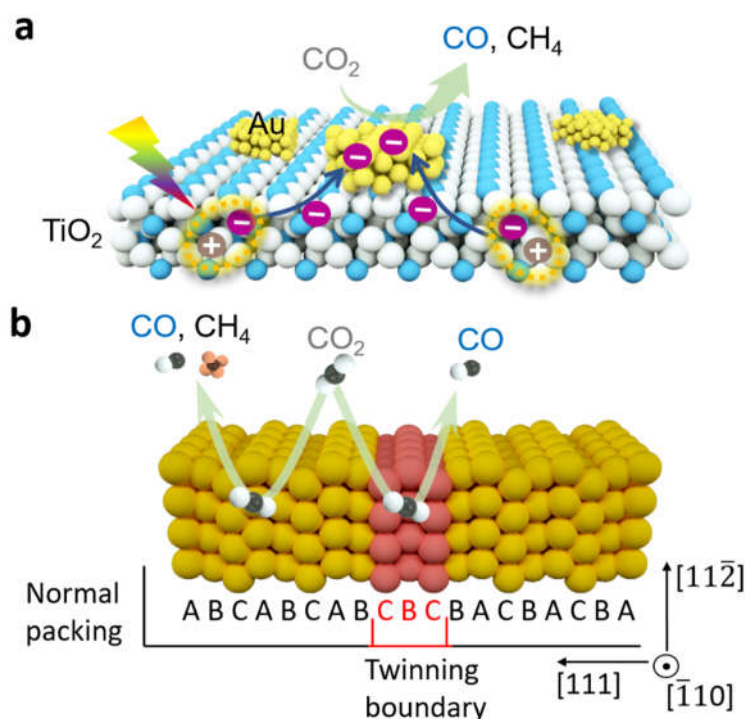

Figure 1. (a) CO_2 photoreduction over the model photocatalyst of Au NPs supported TiO_2. **(b)** Schematic representation of twin stacking fault in Au crystal viewed along the $[\bar{1}10]$ zone axis. The shaded red area highlights the structural and electronic disturbance to normal atomic packing at the twin boundary surface.

Herein, we proposed to a phase-doping strategy to regulate the pathway of CO_2 photoreduction by chemically modifying the surface structure of *fcc*-phase Au NPs, i.e. a stacking faults with the ordering of the *fcc* planes in the [111] direction (Figure 1b), and demonstrated a new case of materials-gene

engineering to precisely design photocatalytic materials with the prescribed properties. Firstly, we performed the thermodynamic analysis of the CO_2 conversion pathways over the surface of normal *fcc*-phase and twinning phase Au NPs with density functional theory (DFT). The potential energy diagrams of CO_2-to-CO and CO_2-to-CH_4 pathways were represented in Figure 2 and S1 (see supporting information). The positive energy barrier of +0.81 eV further indicated that the two-electron reduction of CO_2 to CO remains a thermodynamically non-spontaneous process even through the PCET pathway, while the negative energy barrier of -1.56 eV showed that the eight-electron reduction of CO_2 to CH_4 is thermodynamically-permitted under ambient conditions (Figure 2a-d). The high adsorption energy of the *COOH intermediate led to a large Gibbs energy barrier of +1.848 eV over the *fcc*-Au (110) facet and +2.05 eV over the *fcc*-Au (100) facet, which is the most crucial point to block CO production at high efficiency and selectivity. In contrast, a low Gibbs energy barrier of +0.328 eV was demanded for the *HCOO formation ($CO_2 + H^+ + e^- \rightarrow$ *HCOO, Eq. 3) over the *fcc*-Au (110) facet, lower than that (+0.730 eV) over the *fcc*-Au (100) facet. These thermodynamic analysis results clearly indicated that the (110) facet is more active for the CO_2 reduction than the (100) facet. The charge density difference profiles represented in (Figure S2a and b, see supporting information) further corroborated the above-mentioned conclusion. The strong localization of charges around the *COOH adsorbate indicated that the CO_2-to-CO conversion was limited by the poor chemical affinity of surface Au atoms to the key intermediate.
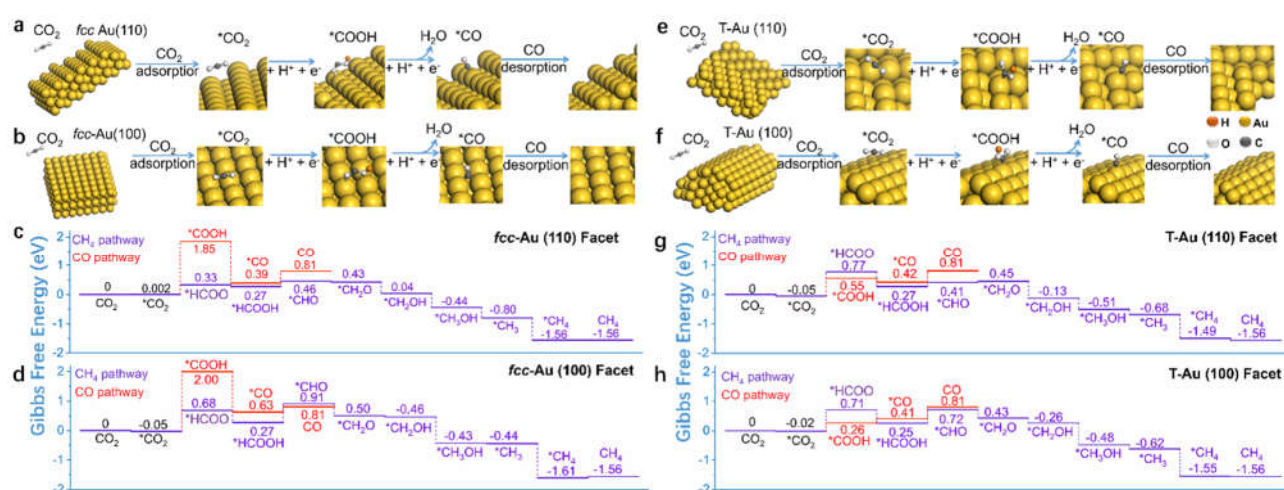

Figure 2. The adsorption configurations of CO_2 and reactive intermediates of CO generation over the (110) (**a**) and (100) (**b**) planes of *fcc*-Au. The potential energy diagrams of the CO_2 conversion over

the (110) (**c**) and (100) (**d**) planes of *fcc*-Au. The adsorption configurations of CO_2 and reactive intermediates of CO generation over the (110) (**e**) and (100) (**f**) planes of T-Au. The potential energy diagrams of the CO_2 conversion over the (110) (**g**) and (100) (**h**) planes of T-Au.

Amazingly, it was found that the thermodynamic confinement can be unlocked with the twinning-phase Au (T-Au) NPs. Due to the pronounced changes on the atomic configuration and surface energy of the twinned (110) and (100) planes (Figure 2e and f),[7] An opposite energetic trend was exhibited over the T-Au (110) facet, as displayed in Figure 2g. The energy barrier of *HCOO (+0.82 eV) was larger than that of *COOH (+0.60 eV). Also, the T-Au (100) facet yielded similar findings (Figure 2h). The adsorption energy of *COOH (+0.26 eV) was lower than that of *HCOO (+0.71 eV eV). These findings indicated clearly that the T-Au (110) and (100) facets were far more beneficial for CO production, compared to the regular *fcc*-Au packed surfaces. Given the fact that CO can act as an intermediate to generate CH_4 (CO → COH → C → …→CH_4), [8] the desorption energy of CO on the catalyst surface will consequently determine if CO is an intermediate, or ends up being the final product. The Gibbs energy of the *COH formation over the T-Au (110) and (100) facets are1.07 and 1.00 eV, respectively, which are markedly larger than the desorption energies of the CO molecules on each surface, 0.39 eV of T-Au (110) and 0.40 eV of T-Au (100) (Figure S3, see Supporting Information). These DFT calculations suggested that the T-Au is more beneficial for the desorption of CO molecules from the catalyst surface than for the protonation of *CO to produce *COH and finally form CH_4. This was mainly originated from the giant change in adsorption configuration of *COOH intermediate over the catalyst surface. As represented by the charge density difference profiles (Figure S2c and d), the C atom of *COOH, instead of one of the O atoms, was strongly coordinated to Au with a bond length of 2.09 ± 0.01Å, which made the charges delocalized at a large-range, especially over the T-Au (100) facet. The results showed that the pathway of CO_2 conversion is highly sensitive to the surface structure of Au NPs, and thus inspired us to incorporate the twining phase into the normal *fcc*-phase Au NPs for achieving the target conversion at high selectivity.

Next, in light of the above-mentioned theoretical predictions, a series of twinned Au NPs modified TiO_2 (x-T-Au/TiO_2, x denotes the Au weight percentage) and a conventional face-centered cubic Au/TiO_2 (x-*fcc*-Au/TiO_2) were prepared (see Methods for details) by a one-step chemical reduction method for the *in situ* growth of twinned Au NPs (T-Au; *fcc* structures doped by multiple twinning

planes) on TiO$_2$ as cocatalyst for the efficient and selective photoreduction of CO$_2$ to CO under simulated solar illumination. The real content of Au in 5-T-Au/TiO$_2$ and 5-*fcc*-Au/TiO$_2$ were determined by inductively coupled plasma optical emission spectrometry (Table S1, see Supporting Information). The crystal structure of the as-prepared T-Au/TiO$_2$ materials were characterized by synchrotron-based powder X-ray diffraction (Figure S4, see Supporting Information), revealing the TiO$_2$ component to possess a mixture of anatase and rutile phases. [9] With increasing Au loading (from 0-15%), the Au NPs introduced additional peaks which are well-assigned to its cubic crystal structure. X-ray photoelectron spectra confirmed the metallic Au^0 state found in both 5-*fcc*-Au/TiO$_2$ and 5-T-Au/TiO$_2$ (Figure S5, see Supporting Information), [10] but the phase-doping made the Au-plasmon band red-shifted by 9 nm (Figure S6, see Supporting information).

Figure 3. (**a**) TEM and (**b**) HRTEM of 5-T-Au/TiO$_2$ (**c**) HRTEM and scheme of T-Au, corresponding to the enlarged area identified in (**b**). (**d**) Corresponding indexed 2D fast Fourier transform of [0$\bar{1}\bar{1}$] (red) and [011] (white) extracted from the T-Au imaged in (**c**).

Transmission electron microscopy (TEM: Figure 3a and S7) resolved the crystalline structure of the T-Au NPs. High-resolution micrographs (HRTEM: Figure 3b and c) showed the typical lattice parameter

of 0.23 nm, corresponding to the inter-planar spacing between (111) planes of Au. Enlarging the image (Figure 3c), two ABCBCBA stacking sequences corresponding to twinning planes were indexed in the T-Au particle, manifesting as peak splitting in the indexed Fast-Fourier transform (FFT) patterns of the HRTEM image (Figure 3d). This confirmed that the lattice possesses a BCB stacking sequence and a twin-symmetry of the intertwined particles.[7] Furthermore, these two sets of diffraction patterns with an interval angle of 110.5° suggested the rotation of lattice plane along the $[\bar{1}1\bar{1}]$ direction, governed by a $[\bar{1}1\bar{1}]$ twinning plane. Meanwhile, in the HRTEM image of T-Au/TiO_2, the normal *fcc* stacking, ABCABC, was resolved without twinning signatures. [7] For completeness, the TEM and HRTEM images of *fcc*-Au/TiO_2 were presented in Figure S8 (see Supporting Information), where only a pure *fcc* phase can be observed in the Au particles. The size of the Au NPs in both *fcc*-Au/TiO_2 and T-Au/TiO_2, as determined from HRTEM, were comparable (*ca*. 13 nm; Figure S9, see Supporting Information).

The photocatalysts were tested for the CO_2 photoreduction with H_2O under simulated solar light. After 4 h illumination (Figure 4a), pure TiO_2 produced on average 16.8 µmol g^{-1} h^{-1} CO and 3.1 µmol g^{-1} h^{-1} CH_4, or an 84% selectivity towards CO. TiO_2 decorated with T-Au NPs had a significantly higher CO production. 1-T-Au/TiO_2 for example, with 1 wt% T-Au, displayed 335 µmol g^{-1} h^{-1} CO or a ca. 20-fold enhancement, while only traces of CH_4 (9.3 µmol g^{-1} h^{-1}) were produced corresponding to a 97 % CO selectivity. The best photocatalytic performance was obtained for 5-T-Au/TiO_2 with a CO yield rate of 608 µmol g^{-1} h^{-1}, which is approximately 40 times higher than that of pristine TiO_2. This CO yield rate is relatively high among reported Au-based photocatalysts (Table S2, see Supporting Information). The apparent quantum yield of CO production was measured to be 0.2% at 380 nm. Due to the minute amounts of CH_4 (8.7 µmol g^{-1} h^{-1}) produced, this photocatalyst also had an excellent CO selectivity nearing 99 %. Although the Au is a noble metal, the cost-effectiveness over T-Au/TiO_2 is much higher than the pristine TiO_2, that ca. 12.8-fold increase in photocatalyst cost can bring about *ca*. 40-fold increase in activity. The 5-*fcc*-Au/TiO_2 photocatalyst also displayed a decent CO_2 reduction activity with 305 µmol g^{-1} h^{-1} CO and 102 µmol g^{-1} h^{-1} CH_4. However, a low CO selectivity of 75% was achieved. As revealed by DFT calculations, CH_4 was a more favored product than CO over *fcc*-Au, but CH_4 generation needed 8 electrons and a much longer reaction dynamic process in comparison to CO generation. Thus, it was reasonable to assume that CH_4 and CO can be generated on the *fcc*-Au

surface, simultaneously, and was in fact observed experimentally. Furthermore, compared to pristine TiO_2, the selectivity of CH_4 has been boosted from 16% to 25% in *fcc*-Au/TiO_2. Control experiments (Table S3, see Supporting Information) e.g. with $^{13}CO_2$ confirm that the generated CO originates from CO_2 photoreduction (Figure S10, see Supporting Information). T-Au and *fcc*-Au without a TiO_2 support for CO_2 photoreduction were also tested (Table S3), whereby only trace CO and CH_4 were generated over both (too low to be detected reliably). Similarly, the amount of CO and CH_4 generated was also too low to be detected over 5-T-Au/TiO_2 and 5-*fcc*-Au/TiO_2 under visible light irradiation (> 420 nm; Table S3). These findings indicated that TiO_2 is the solar absorber to generate and transport photo-carriers to the Au NPs, which acted as a cocatalyst to improve the catalytic performance. The best performing 5-T-Au/TiO_2 also showed a stable performance during consecutive cycles (Figure 4b). After 12 h, no decrease in activity or CO selectivity was observed. HRTEM further confirmed the stability of the twinning planes in 5-T-Au/TiO_2 (Figure S11, see Supporting Information). H_2O_2, instead of O_2, was generated as the oxidation products over T-Au/TiO_2, which we detect using *in-situ* Fourier-transform infrared (FTIR) spectroscopy (Figure S12, see Supporting Information).

Figure 4c and 4d respectively demonstrated *in-situ* FTIR spectra of the 5-*fcc*-Au/TiO_2 and 5-T-Au/TiO_2 surfaces with simulated solar light irradiation to directly detect the reaction intermediates of CO_2 reduction. The absorption peak at 1331 cm^{-1} belonging to a HCOO* group was resolved in 5-*fcc*-Au/TiO_2,[11] which is the key intermediate for the CH_4 generation as revealed by DFT in Figure 2. For photoreduction over 5-T-Au/TiO_2, the HCOO* cannot be indexed. In comparison to 5-T-Au/TiO_2, 5-*fcc*-Au/TiO_2 was more favorable for the CH_4 generation. The strong band near 1715 cm^{-1} in 5-T-Au/TiO_2 can be assigned to the surface bonded COOH* which is the crucial intermediate for CO generation.[12] This band was much weaker in the 5-*fcc*-Au/TiO_2. Conversely, the intensity of CO* vibration around 2065 cm^{-1} in 5-*fcc*-Au/TiO_2 was stronger than that in 5-T-Au/TiO_2. It can be attributed to the fact that CO* was easier to desorb from the 5-T-Au/TiO_2 surface. These *in situ* FTIR results verified the above-mentioned theoretical predictions.

To further unravel the origin of the enhanced photocatalytic activity, the optoelectronic and texture properties of 5-*fcc*-Au/TiO_2 and 5-T-Au/TiO_2 were evaluated. No intrinsic relationship can be established between the enhancement of photocatalytic activity and changes in texture properties (Figure S13 and Table S4, see Supporting Information), whereas the photoluminescence and on-off

photocurrent results (Figure S14-16, see Supporting Information) showed that a more efficient transfer of photo-generated electrons from TiO_2 to Au NPs was achieved in the 5-T-Au/TiO_2 compared to 5-*fcc*-Au/TiO_2. The CO_2 adsorption isotherms in Figure S17 (see Supporting Information) suggest the smaller CO_2 adsorption capacity in 5-T-Au/TiO_2 than that of 5-*fcc*-Au/TiO_2. This is attributed to the fact that hydrophilicity of 5-T-Au/TiO_2 is better than that of 5-*fcc*-Au/TiO_2 sample (Figure S18, see Supporting Information) and the more water adsorption on the 5-T-Au/TiO_2 surface, thus leading to less surface-active sites reserved for the CO_2 molecules adsorption and then low CO_2 adsorption capacity. Moreover, the significant increase in chemical affinity to polar H_2O molecules over 5-T-Au/TiO_2 catalyst as compared with 5-*fcc*-Au/TiO_2 sample gives the evidence for the strong adsorption capacity to polar COOH* intermediate. The temperature-programmed desorption (TPD) profiles (Figure S19, see Supporting Information) presented a lower CO desorption peak centered at ca. 400 °C and a higher CH_4 desorption temperature of 400 °C on 5-T-Au/TiO_2, compared to 5-*fcc*-Au/TiO_2 (410 ℃ for CO-TPD and 360 ℃ for CH_4-TPD). All these results directly supported the notion that CO is released easier on the T-Au/TiO_2 surface, which is consistent to the above-mentioned FTIR results.
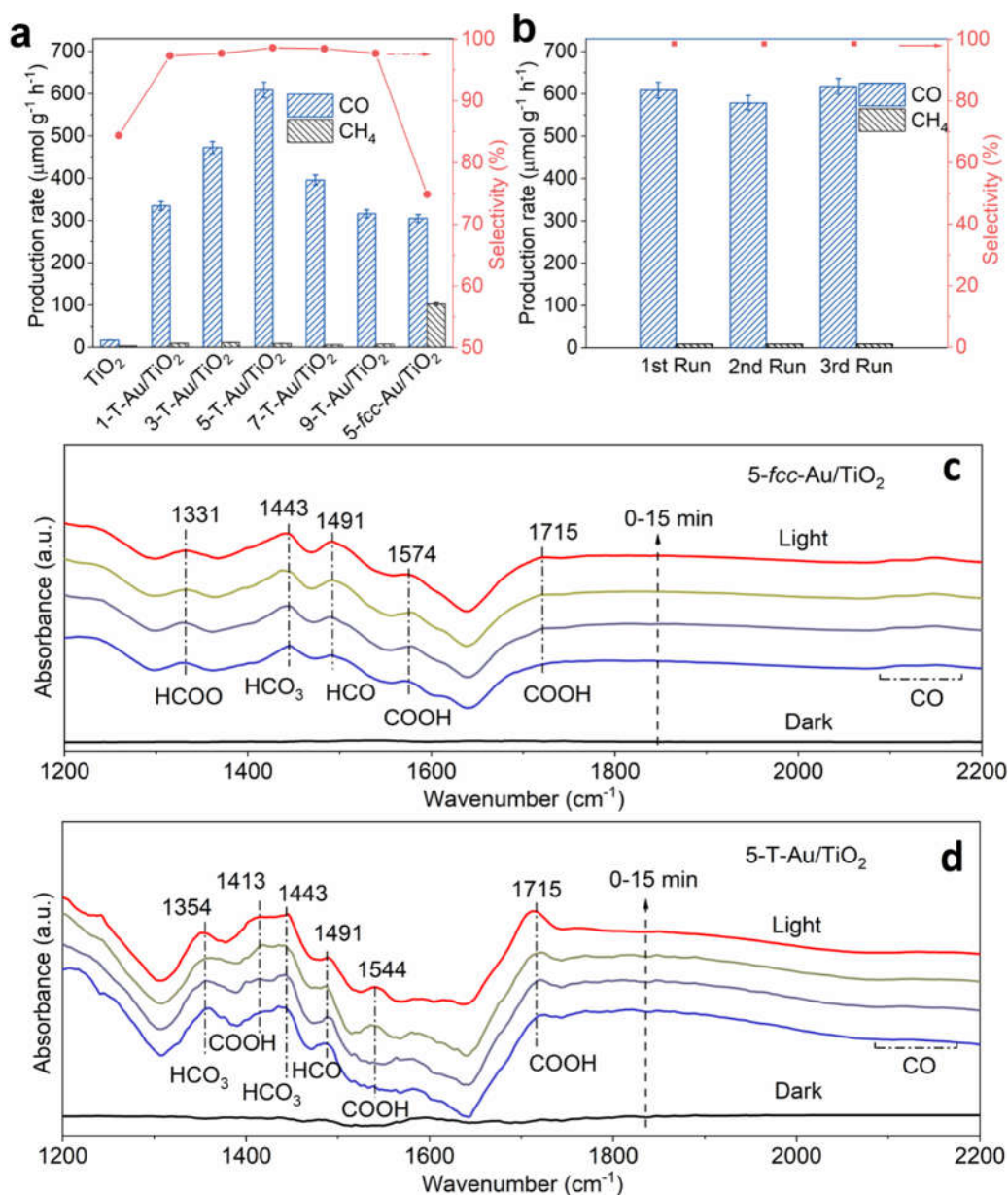
Figure 4. (**a**) CO_2 Photocatalytic reduction over pure TiO_2, x-T-Au/TiO_2 and 5-fcc-Au/TiO_2; (**b**) Recycle test for 5-T-Au/TiO_2; *In situ* FTIR spectra for co-adsorption of a mixture of CO_2 and H_2O vapour on 5-*fcc*-Au/TiO_2 (**c**) and 5-T-Au/TiO_2 (**d**).

In summary, the thermodynamic bottleneck of CO_2-to-CO conversion was unlocked by the phase incorporation of twinning planes into normal *fcc*-phase Au NPs. The as-prepared T-Au NPs could act as not only an electron sink to extract the photogenerated electrons in the TiO_2, but also the reaction site for CO_2 reduction. A nearly 40-fold enhancement in CO_2 reduction activity was achieved on T-Au/TiO_2 compared to pristine TiO_2. Unlike the *fcc*-Au modified TiO_2, the T-Au/TiO_2 presented a near 100% selectivity to CO. As reveled by experimental and theoretical studies, the high CO selectivity on

T-Au/TiO_2 was attributed to the low energy barrier for CO generation and easy desorption on the surface of twinned Au NPs. In a word, this work not only extended the twinning defect engineering option available for gold photocatalysis and offered a promising avenue for CO_2 photoreduction, but also offered a hint that the twinning Au plasmonic photocatalysts with diverse properties can be used to synthesize the different target products with solar energy.

Acknowledgements

Keywords: Phase doping • Twinning defects • Gold photocatalysis • CO_2 reduction • Materials gene engineering

[1] X. Chang, T. Wang, J. Gong, *Energy Environ. Sci.* 2016,9, 2177-2196.

[2] a) X. Jiao, K. Zheng, L. Liang, X. Li, Y. Sun, Y. Xie, *Chem. Soc. Rev*. 2020, 49, 6592-6604; b) Y. Li, J. Hao, H. Song, F. Zhang, X. Bai, X. Meng, H. Zhang, S. Wang, Y. Hu, J. Ye, *Nat. Commun.,* 2019, 10, 2359.

[3] a) F. Farshchi Tabrizi, S. A. H. S. Mousavi, H. Atashi, *Energy Convers. Manage.* 2015, 103, 1065-1077; b) E. D. Goodman, A. A. Latimer, A. Yang, L. Wu, N. Tahsini, F. Abild-Pedersen, M. Cargnello *ACS Appl. Nano Mater.* 2018, 1, 5258-5267.

[4] a) X. Li, J. Yu, M. Jaroniec, X. Chen, *Chem. Rev.,* 2019, 119, 3962-4179; b) J. Fu, K. Jiang, X. Qiu, J. Yu, M. Liu, *Mater. Today* 2020, 32, 222-243; c) C. Xie, Z. Niu, D. Kim, M. Li, P. Yang *Chem. Rev.*

2020, 120, 1184–1249.

[5] a) X. Jiao, K. Zheng, Q. Chen, X. Li, Y. Li, W. Shao, J. Xu, J. Zhu, Y. Pan,   Y. Sun, Y. Xie, *Angew. Chem. Int. Ed.* 2020, 59, 15497-15501; *Angew. Chem.* 2020, 132, 15627-15631; b) J. Albero, Y. Peng, H. García *ACS Catal.* 2020, 10, 5734-5749.

[6] a) L. Meng, Z. Chen, Z. Ma, S. He, Y. Hou, H. Li, R. Yuan, X. Huang, X. Wang, X. Wang, J. Long, *Energy Environ. Sci.,* 2018, 11, 294-298; b) J. Long, H. Chang, Q. Gu, J. Xu, L. Fan, S. Wang, Y. Zhou, W. Wei, L. Huang, X. Wang, P. Liu, W. Huang, *Energy Environ. Sci.*, 2014, **7**, 973-977; c) D. A. Panayotov, A. I. Frenke, J. R. Morris, *ACS Energy Lett.* 2017, 2, 1223–1231

[7] a) J. Wu, L. Qi, H. You, A. Gross, J. Li, H. Yang, *J. Am. Chem. Soc.* 2012, 134, 11880-11883; b) W. Niu, J. Liu, J. Huang, B. Chen, Q. He, A. Wang, Q. Lu, Y. Chen, Q. Yun, J. Wang, C. Li, Y. Huang, Z. Lai, Z. Fan, X. Wu, H. Zhang. *Nat. Commun.* 2019, 10, 2881; c) M. Krajci, S. Kameoka, A.-P. Tsai, *J. Chem. Phys.* 2017, 147, 044713.

[8] a) J. Zhao, B. Liu, L. Meng, S. He, R. Yuan, Y. Hou, Z. Ding, H. Lin, Z. Zhang, X. Wang, J. Long, *Appl. Catal. B Environ.,* 2019, 256, 117823; b) S.N. Habisreutinger, L. Schmidt-Mende, and J. K. Stolarczyk, *Angew. Chem. Int. Ed.*, 2013, 52, 7372-7408; *Angew. Chem.* 2013, 125, 7516-7557.

[9] A. Fujishima, X. Zhang, D. A. Tryk, *Surf. Sci. Rep.* 2008, 63, 515-582

[10] D. Ding, K. Liu, S. He, C. Gao, Y. Yin, *Nano Lett.* 2014, 14, 6731-6736

[11] a) S. Zhu, T. Li, W. Cai, M. Shao, *ACS Energy Lett.* 2019, 4, 682-689; b) X. Li, Y. Sun, J. Xu, Y. Shao, J. Wu, X. Xu, Y. Pan, H. Ju, J. Zhu, Y. Xie, *Nat. Energy* 2019, 4, 690-699; M. Dunwell, Y. Yan, B. Xu, *ACS Catal.* 2017, 7, 5410-5419.

[12] K. Jiang, J. Chang, H. Wang, S. Brimaud, W. Xing, R. J. Behm, W-B. Cai, *ACS Appl. Mater. Interfaces* 2016, 8, 7133–7138